Journal of Sound and Vibration (2000) **235**(3), 435–449
doi:10.1006/jsvi.2000.2937, available online at http://www.idealibrary.com on IDEAL®

NON-LINEAR FUZZY LOGIC CONTROL FOR FORCED LARGE MOTIONS OF SPINNING SHAFTS

SHULIANG LEI, ALAN PALAZZOLO AND UHNJOO NA

Texas A&M University, Department of Mechanical Engineering, College Station, TX 77843-3123, *U.S.A.*

AND

ALBERT KASCAK

U.S. Army at NASA Lewis, 21000 *Brookpark RD, Cleveland, OH* 44135, *U.S.A.*

(*Received* 3 *September* 1999, *and in final form* 7 *February* 2000)

A unique control approach is developed for prescribed large motion control using magnetic bearings in a proposed active stall control test rig. A finite element based, flexible shaft is modeled in a closed loop system with PD controllers that generate the control signals to support and to shake the rotor shaft. A linearized force model of the stall rig with 16 magnetic poles (4 opposing C-cores) yields stability and frequency responses. The non-linear model retains the non-linearities in Ampere's law, Faraday's law and the Maxwell stress tensor. A fuzzy logic control system is then designed to show the advantages over the conventional controllers with the fully non-linear model.

1. INTRODUCTION

In recent years, the use of magnetic bearings in rotating machinery has received much interest due to its potential advantages. Active magnetic bearings (AMB) offer a way to both support the rotating shaft as well as to control vibration. Most magnetic bearings utilize a linear PID controller with power amplifiers, magnetic actuators and inductive, eddy current or optical sensors [1, 2]. These electronic components act linearly up to a saturation limit. The linear controller usually does not include logic for maintaining accurate control with non-linear system behavior.

To suppress rotating stall in a high-speed compressor wheel, it is desired to shake the wheel at a large amplitude while maintaining the rotor system stable. Electromagnetic shakers and magnetic bearings have been used for actuators in a majority of vibration control. A lot of work was done on the control of AMB system using conventional methods. Beside the basic PID controller, some advanced control strategies, such as optimal control [3, 4], μ-synthesis control [5], H_∞ control [6–8], have also been employed in the study of magnetic bearings. However, these advanced control techniques require a linear model. In many cases, the linear model fails to approximate the practical plant and the above advanced control methods cannot be applied.

In the case of a magnetic shaker with the non-linear models, there are some difficulties to obtain large whirl orbits because of system instability. By carefully designing a PD controller the shaking orbit radius can be increased but only to a limited value in the stable region.

0022-460X/00/330435 + 15 $35.00/0

Motivated by the capability of dealing with non-linearities of the problem, fuzzy logic has been introduced for control of magnetic bearing system. Fuzzy logic theory was first established in Zadeh's seminal paper [9] in 1965. Since then it has been considered as an effective means in various control problems. An idea of applying fuzzy logic to dynamics systems was introduced in early 1970s by Mamdani [10]. The Mamdani architecture of fuzzy logic controller is build up based on qualitative and empirical knowledge of human beings. Later Takagi and Sugeno established a fuzzy model [11], called Takagi–Sugeno model, which can be more easily used for analytical purpose.

The AMB non-linear model considers the three cases: non-linear *B-H* curve, Ampere's law and Maxwell stress tensor. Fuzzy logic control is constructed by designing a rule base to implement a non-linear control strategy. The antecedent and consequent of each rule operate on the positions of input and output variables in predefined membership functions. These membership functions possess qualitative descriptions which generalize the notion of assigning a single degree to a specific response severity or corrective action level. Research in the area of AMB using fuzzy logic control is mainly based on a simple model such as lumped mass model or rigid-body model [12, 13]. Some application needs to recursively tune the rules to achieve better performances [14]. While these results are absorbing, they cannot deal with a flexible shaft with a dimension of over hundreds of structural states plus control variables. The stall-rig model consists of a rotating shaft with a compressor wheel. The finite element method is used to describe the flexible rotor in designing a suitable control and analyzing the system behavior. The front bearing is an active magnetic bearing system, which includes feedback between non-collocated sensors and actuators, via controllers. The shaft is divided into 23 elements, and at node 17, an oil-film bearing is employed to support the rotor system. The magnetic bearing is located at node 9. The non-collocated sensors are placed at node 7 and have output-directed PD controllers. The control signals are then directed to power amplifiers to produce control currents, which drive the coils of the magnetic bearings to control the rotor system. The shaking voltages are applied to a summing point at the control output to force the shaft to execute motions that alter the compressor wheel's tip clearance and inhibit stall cell formation.

Fuzzy logic controllers for active magnetic bearings are synthesized and designed for suppression of imbalance vibration and to increase the shaking orbit radius. The main objective of this paper is to develop robust controllers for maintaining magnetic bearing system stability against imbalance and external shaking forces or voltages for linear and non-linear models. Applying the basic magnetic bearing theory yields a fully non-linear model. Based on the non-linear magnetic bearing model, linearization is carried out to formulate a complete linear model for analysis. The PD controller and the fuzzy logic controllers based on Mamdani architecture are synthesized and designed. The superiority of non-linear fuzzy logic control over linear PD control is also shown. Simulation results for each type of controllers are provided and their performance specifications can be compared accordingly.

2. SYSTEM MODEL

2.1. MAGNETIC BEARING FORCE

Consider the two opposing magnetic C-cores shown in Figure 1. According to Ampere's law, the magnetic flux ϕ^+ in the positive C-core is

$$\phi^+ = \frac{(N_B i_B + N_c i)}{2w^+}\mu_0 A_a = \frac{(N_B i_B + N_c i)}{2(g_0 - w)}\mu_0 A_a. \tag{1}$$

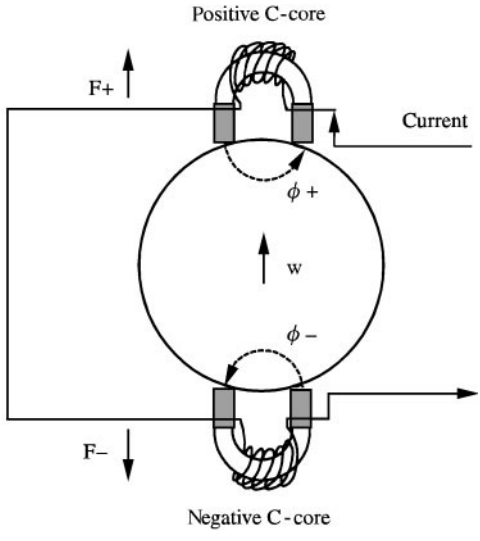

Figure 1. Schematic of two opposing C-cores.

The magnetic flux ϕ^- in the negative C-core is

$$\phi^- = \frac{(N_B i_B - N_c i)}{2w^-}\mu_0 A_a = \frac{(N_B i_B - N_c i)}{2(g_0 + w)}\mu_0 A_a, \tag{2}$$

where g_0 is the air gap of the magnetic bearing and w is the displacement of the rotor in positive direction. The corresponding flux density in the positive magnetic path and the negative magnetic path can then be written as

$$B^+ = \frac{\phi^+}{A_a} = \frac{(N_B i_B + N_c i)}{2(g_0 - w)}\mu_0, \qquad B^- = \frac{\phi^-}{A_a} = \frac{(N_B i_B - N_c i)}{2(g_0 + w)}\mu_0. \tag{3}$$

Note that Ampere's law yields flux expressions that are non-linear functions of the shaft displacement w.

A second non-linearity occurs when the Maxwell stress tensor formula is applied to obtain the resultant electromagnetic force of the two opposing C-cores:

$$F = \left[(B^+)^2 \frac{A_a}{\mu_0} - (B^-)^2 \frac{A_a}{\mu_0}\right] \cos\delta, \tag{4}$$

where

$$(B^+)^2 = \frac{(N_B i_B + N_c i)^2}{4(g_0 - w)^2}\mu_0^2, \qquad (B^-)^2 = \frac{(N_B i_B - N_c i)^2}{4(g_0 + w)^2}\mu_0^2. \tag{5}$$

This yields

$$F = \eta^2 \cos\delta \frac{A_a \mu_0}{4}\left[\left(\frac{N_B i_B + N_c i)}{g_0 - w}\right)^2 - \left(\frac{N_B i_B - N_c i)}{g_0 + w}\right)^2\right]. \tag{6}$$

The related parameters for the example considered are: $\mu_0 = 4\pi \times 10^{-7}$ (H/m), permeability. $A_a = (6/39{\cdot}37^2)(\mathrm{m}^2)$, area per pole; $g_0 = 0{\cdot}02/39{\cdot}37\,(\mathrm{m})$, air gap; $\delta = 360^\circ/(16 \times 2) = 11{\cdot}25^\circ$, half angle between poles; $\eta = 0{\cdot}9$, derate factor; $i_B = 30\,(\mathrm{A})$, bias current; $N_B = 40$ (turns per C-core), bias coil; $N_c = 16$ (turns per C-core), control coil.

2.2. COIL INDUCTANCE AND VOLTAGE

According to Faraday's law, the coil voltage in each C-core can be written as follows.
Positive C-core:

$$V_L^+ = N_c \frac{\mathrm{d}\phi^+}{\mathrm{d}t} = \frac{N_c^2 \mu_0 A_a}{2} \frac{\mathrm{d}}{\mathrm{d}t}\left(\frac{i}{w^+}\right). \tag{7}$$

Negative C-core:

$$V_L^- = N_c \frac{\mathrm{d}\phi^-}{\mathrm{d}t} = \frac{N_c^2 \mu_0 A_a}{2} \frac{\mathrm{d}}{\mathrm{d}t}\left(\frac{i}{w^-}\right). \tag{8}$$

or

$$\begin{aligned} V_L^+ &= \frac{N_c^2 \mu_0 A_a}{2w^+} \frac{\mathrm{d}i}{\mathrm{d}t} + \frac{N_c^2 \mu_0 A_a}{2} i \frac{\mathrm{d}}{\mathrm{d}t}\left(\frac{1}{w^+}\right) \\ &= L^+ \frac{\mathrm{d}i}{\mathrm{d}t} + \frac{N_c^2 \mu_0 A_a}{2} i \frac{\mathrm{d}}{\mathrm{d}t}\left(\frac{1}{g_0 - w}\right) \end{aligned} \tag{9}$$

and

$$\begin{aligned} V_L^- &= \frac{N_c^2 \mu_0 A_a}{2w^-} \frac{\mathrm{d}i}{\mathrm{d}t} + \frac{N_c^2 \mu_0 A_a}{2} i \frac{\mathrm{d}}{\mathrm{d}t}\left(\frac{1}{w^-}\right) \\ &= L^- \frac{\mathrm{d}i}{\mathrm{d}t} + \frac{N_c^2 \mu_0 A_a}{2} i \frac{\mathrm{d}}{\mathrm{d}t}\left(\frac{1}{g_0 + w}\right), \end{aligned} \tag{10}$$

where

$$L^+ = \frac{N_c^2 \mu_0 A_a}{2}\left(\frac{1}{g_0 - w}\right), \qquad L^- = \frac{N_c^2 \mu_0 A_a}{2}\left(\frac{1}{g_0 + w}\right) \tag{11}$$

are the non-linear inductances of the coils on the two opposing C-cores.

Considering the coil resistance R, the voltage drop across the power amplifier output terminals for two opposing C-cores becomes

$$V = 2Ri + L^+ \frac{\mathrm{d}i}{\mathrm{d}t} + \frac{N_c^2 \mu_0 A_a}{2} i \frac{\mathrm{d}}{\mathrm{d}t}\left(\frac{1}{g_0 - w}\right) + L^- \frac{\mathrm{d}i}{\mathrm{d}t} + \frac{N_c^2 \mu_0 A_a}{2} i \frac{\mathrm{d}}{\mathrm{d}t}\left(\frac{1}{g_0 + w}\right). \tag{12}$$

Equations (10)–(12) show the non-linearity that is contained in the voltage expression obtained from Faraday's law.

2.3. FLUX DENSITY SATURATION

Due to the non-linear property of the ferromagnetic materials, the flux density in the magnetic circuit will saturate with increase of exciting coil current. The AMB forces saturate accordingly due to the saturation of the magnetic field.

For simplicity, suppose the saturation flux density is 2 Tesla:

$$B^{+}_{\max} = B^{-}_{\max} = 2(\text{Tesla}). \tag{13}$$

Then we have for the maximum AMB forces,

$$F^{-}_{\max} = F^{+}_{\max} = \eta^2 \cos\delta (B^{+}_{\max})^2 \frac{A_a}{\mu_0} = 4\eta^2 \cos\delta A_a \mu_0. \tag{14}$$

The saturation of flux density B limits the maximum force

$$F_{\max} = (B^{+}_{\max})^2 \frac{A_a}{\mu_0}. \tag{15}$$

The above result is valid for each opposing C-core pair (two opposing C-cores).

2.4. CLOSED-LOOP SYSTEM

The basic configuration of one control channel is shown in Figure 2.

In this diagram, we use PD controllers in the feedback loop. A more elegant non-linear fuzzy logic controller will be described later. It can be seen from this configuration that the shaft is divided into 23 elements. Dimensional data for this model are given in Appendix A. The sensor is located at node 7 and the actuator is located at node 9: this is a non-collocated system. An oil-film bearing is placed at node 17 to support the other end of the shaft (see Appendix A). The sensor measures the displacement signal of the rotor and feeds the signal to the controller. The controller synthesizes the input signal to generate output voltage to

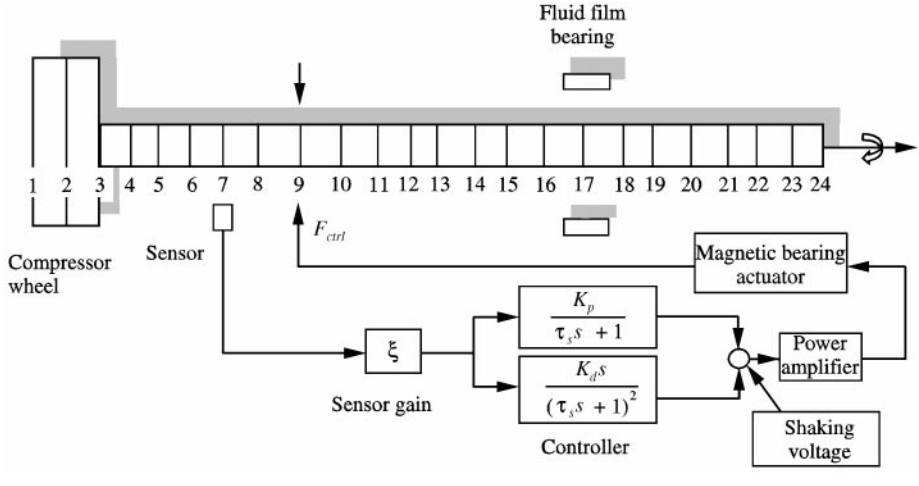

Figure 2. Finite element model of shaft plus feedback control path.

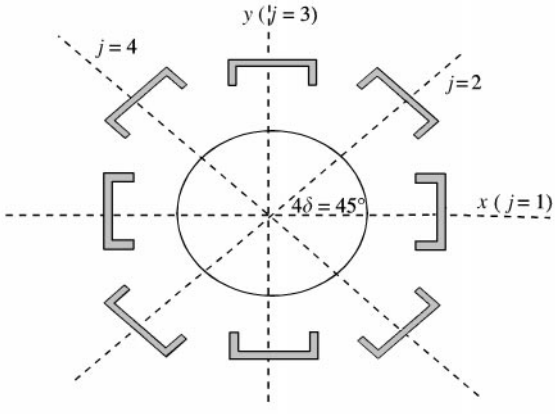

Figure 3. Configuration of the 4 C-core-pairs.

the power amplifier (PA), which in turn produces the control current for the magnetic bearing coil to support the rotor. The compressor wheel is located in the first two elements and the operating rotor spinning rate is set to $\Omega = 17\,000$ rpm.

3. LINEAR ANALYSIS

3.1. LINEARIZATION

The magnetic bearing used to support and shake the rotor has 16 poles, which constitutes 4 C-core-pairs. The four magnetic bearing system consists of 8 C-cores distributed around the circle at uniform angles of 45°. Each C-core has 2 poles, N and S, two opposing C-cores have 4 poles. Totally, the system has 16 poles evenly distributed at an angle of 22·5°. Figure 3 shows the configuration of the 4 C-core-pairs.

Rewrite F for the jth ($j = 1, 2, 3, 4$) C-core pole pair as

$$\begin{aligned} F &= \eta^2 \cos\delta \frac{A_a \mu_0}{4}\left[\left(\frac{N_B i_B + N_c i}{g_0 - w}\right)^2 - \left(\frac{N_B i_B - N_c i}{g_0 + w}\right)^2\right] \\ &= k_\alpha\left[\left(\frac{N_B i_B + N_c i}{g_0 - w}\right)^2 - \left(\frac{N_B i_B - N_c i}{g_0 + w}\right)^2\right], \end{aligned} \tag{16}$$

where

$$k_\alpha = \eta^2 \cos\delta \frac{A_a \mu_0}{4}. \tag{17}$$

Linearize the force at $i = 0$ and $w = 0$:

$$\frac{\mathrm{d}F}{\mathrm{d}i} = 2k_\alpha\left[\frac{(N_B i_B + N_c i)N_c}{(g_0 - w)^2} + \frac{(N_B i_B - N_c i)N_c}{(g_0 + w)^2}\right]\Bigg|_{\substack{i=0\\w=0}} = 4k_\alpha \frac{i_B^2}{g_0^2} N_B N_c, \tag{18}$$

$$\frac{\mathrm{d}F}{\mathrm{d}w} = 2k_\alpha\left[\frac{(N_B i_B + N_c i)^2}{(g_0 - w)^3} + \frac{(N_B i_B - N_c i)^2}{(g_0 + w)^3}\right]\Bigg|_{\substack{i=0\\w=0}} = 4k_\alpha N_B^2 \frac{i_B^2}{g_0^3}. \tag{19}$$

Therefore,

$$\mathbf{F} = [F_x(x, y, i_x, i_y), F_y(x, y, i_x, i_y)]^{\mathrm{T}}$$

$$= \begin{bmatrix} \dfrac{\partial F_x}{\partial g_1} & \dfrac{\partial F_x}{\partial g_2} & \dfrac{\partial F_x}{\partial g_3} & \dfrac{\partial F_x}{\partial g_4} \\ \dfrac{\partial F_y}{\partial g_1} & \dfrac{\partial F_y}{\partial g_2} & \dfrac{\partial F_y}{\partial g_3} & \dfrac{\partial F_y}{\partial g_{41}} \end{bmatrix} \begin{bmatrix} \dfrac{\partial g_1}{\partial x} & \dfrac{\partial g_1}{\partial y} \\ \dfrac{\partial g_2}{\partial x} & \dfrac{\partial g_2}{\partial y} \\ \dfrac{\partial g_3}{\partial x} & \dfrac{\partial g_3}{\partial y} \\ \dfrac{\partial g_4}{\partial x} & \dfrac{\partial g_4}{\partial y} \end{bmatrix} \begin{bmatrix} x \\ y \end{bmatrix} + \begin{bmatrix} \dfrac{\partial F_x}{\partial i_x} & \dfrac{\partial F_x}{\partial i_y} \\ \dfrac{\partial F_y}{\partial i_x} & \dfrac{\partial F_y}{\partial i_y} \end{bmatrix} \begin{bmatrix} i_x \\ i_y \end{bmatrix}. \tag{20}$$

Geometric consideration of the 4 C-core pairs gives the roter displacement in the four directions

$$\begin{aligned} g_1 &= x, \quad g_2 = x\cos(\pi/4) + y\sin(\pi/4), \\ g_3 &= y, \quad g_4 = x\cos(3\pi/4) + y\sin(3\pi/4). \end{aligned} \tag{21}$$

Then,

$$\mathbf{F} = [F_x(x, y, i_x, i_y), F_y(x, y, i_x, i_y)]^{\mathrm{T}}$$

$$= \begin{bmatrix} \dfrac{\partial F_x}{\partial g_1} & \dfrac{\partial F_x}{\partial g_2} & \dfrac{\partial F_x}{\partial g_3} & \dfrac{\partial F_x}{\partial g_4} \\ \dfrac{\partial F_y}{\partial g_1} & \dfrac{\partial F_y}{\partial g_2} & \dfrac{\partial F_y}{\partial g_3} & \dfrac{\partial F_y}{\partial g_4} \end{bmatrix} \begin{bmatrix} 1 & 0 \\ \sqrt{2}/2 & \sqrt{2}/2 \\ 0 & 1 \\ -\sqrt{2}/2 & \sqrt{2}/2 \end{bmatrix} \begin{bmatrix} x \\ y \end{bmatrix} + \begin{bmatrix} \dfrac{\partial F_x}{\partial i_x} & \dfrac{\partial F_x}{\partial i_y} \\ \dfrac{\partial F_y}{\partial i_x} & \dfrac{\partial F_y}{\partial i_y} \end{bmatrix} \begin{bmatrix} i_x \\ i_y \end{bmatrix}. \tag{22}$$

After algebraic manipulations,

$$\mathbf{F} = \mathbf{K}_{pos} \begin{bmatrix} 1 & 0 \\ 0 & 1 \end{bmatrix} \begin{bmatrix} x \\ y \end{bmatrix} + \begin{bmatrix} \dfrac{\partial F_x}{\partial i_x} & \dfrac{\partial F_x}{\partial i_y} \\ \dfrac{\partial F_y}{\partial i_x} & \dfrac{\partial F_y}{\partial i_y} \end{bmatrix} \begin{bmatrix} i_x \\ i_y \end{bmatrix}, \tag{23}$$

where $K_{pos} = 8k_\alpha(i_B^2/g_0^3)N_B$ is the position stiffness.

For the current stiffness, note that

$$\begin{aligned} i_1 &= i_x, \quad i_2 = i_x\cos(\pi/4) + i_y\sin(\pi/4), \\ \mathrm{i}_3 &= i_y, \quad i_4 = i_x\cos(3\pi/4) + i_y\sin(3\pi/4). \end{aligned} \tag{24}$$

Therefore,

$$\begin{bmatrix} \dfrac{\partial F_x}{\partial i_x} & \dfrac{\partial F_x}{\partial i_y} \\ \dfrac{\partial F_y}{\partial i_x} & \dfrac{\partial F_y}{\partial i_y} \end{bmatrix} = N_B N_c 8k_\alpha \frac{i_B}{g_0^2} \begin{bmatrix} 1 & 0 \\ 0 & 1 \end{bmatrix}, \tag{25}$$

where $K_i = N_B N_c 4k_\alpha(i_B/g_0^2)$ is the current stiffness.

The total linearized resultant force is

$$\mathbf{F} = \mathbf{K}_{pos}\begin{bmatrix}1 & 0\\ 0 & 1\end{bmatrix}\begin{bmatrix}x\\ y\end{bmatrix} + \mathbf{K}_i\begin{bmatrix}1 & 0\\ 0 & 1\end{bmatrix}\begin{bmatrix}i_x\\ i_y\end{bmatrix}. \tag{26}$$

To obtain the linear electric load, we ignore the coil inductance difference in the two opposing C-cores due to the radial displacement of the rotor, that is, let

$$w^+ = w^- = g_0.$$

Then $L^+ = L^- = L$, where

$$L = \frac{N_c^2 \mu_0 A_a}{2g_0}. \tag{27}$$

For two opposing C-cores, the linear electric load is

$$V = 2Ri + 2L\,\mathrm{d}i/\mathrm{d}t. \tag{28}$$

3.2. STABILITY AND STEADY-STATE ANALYSIS

The linearized closed-loop equation is expressed as

$$\dot{\mathbf{Z}} = \mathbf{A}\mathbf{Z} + \mathbf{B}\mathbf{u}, \tag{29}$$

where $\mathbf{Z} = [x_1 y_1 \theta_{x1} \theta_{y1} x_2 y_2 \theta_{x2} \theta_{y2} \ldots x_N y_N \theta_{yN} \theta_{zN}]^{\mathrm{T}}$ is the state variable vector of the closed-loop system, **Bu** represents external disturbances, i.e., imbalance and shaking input, and **A** is the closed-loop system matrix where the feedback control forces are included. The system stability property is determined by the eigenvalues of the closed-loop system matrix A. If all the real parts of the eigenvalues of A are negative, i.e., the complex eigenvalues are all located on the left half plane, the system is stable. For a stable system, the steady state solution is given as

$$U = \hat{U}\mathrm{e}^{\mathrm{j}\omega t},$$

where ω is the shaking frequency. This leads to

$$\hat{U}\mathrm{j}\omega\mathrm{e}^{\mathrm{j}\omega t} = A\hat{U}\mathrm{e}^{\mathrm{j}\omega t} + \hat{F}\mathrm{e}^{\mathrm{j}\omega t} \Rightarrow \mathrm{j}\omega\hat{U} = A\hat{U} + \hat{F} \Rightarrow (\mathrm{j}\omega - A)\hat{U} = \hat{F} \Rightarrow \hat{U} = (\mathrm{j}\omega - A)^{-1}\hat{F}.$$

Figure 4 shows the amplitude of the compressor wheel (node 2 and node 9) with respect to the shaking frequency.

The frequency responses are obtained for the following conditions. The shaking frequency varies from 20 to 600 Hz; shaking voltage = 66 V. For the rear bearing (node 17) the oil film bearing has the parameters: $Kyy = 3157308$, $Kyz = 3497545$, $Kzy = -898997$, $Kzz = 1220680$, $Cyy = 1596$, $Cyz = 362$, $Czy = 386$, $Czz = 615$. The rotor spinning rate $\Omega = 17000$ rpm.

Table 1 details the steady state displacements in the x and y directions at node 2, node 5, node 9 and node 17, when the shaking frequency = 200 Hz, respectively.

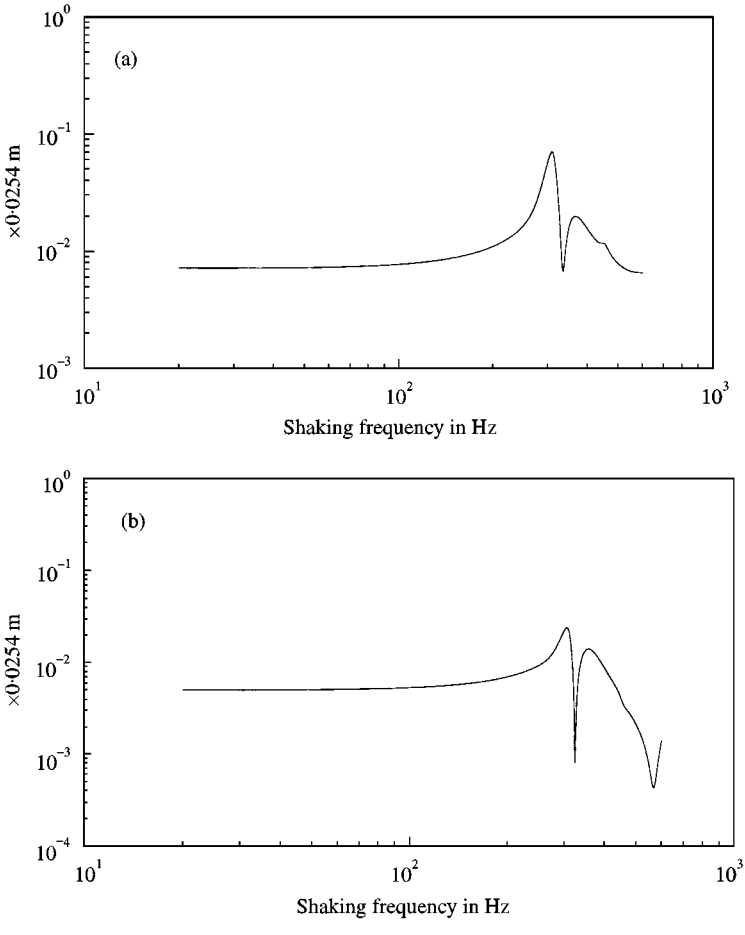

Figure 4. Compressor wheel amplitude vs. shaking frequency: (a) Y direction at node 2 (compressor wheel); (b) Y direction at node 9 (magnetic bearing).

TABLE 1

Steady state displacements

Node number	2	5	9	17
Displacement (mm)	0·292	0·241	0·178	0·0355

Note that this is a linear response prediction and the non-linear response amplitudes were less than 0·25 mm.

4. TRANSIENT RESPONSE SIMULATION WITH PD CONTROLLERS

The simulation was carried out with the following parameters.

PD controllers: proportional control path, $K_p/(\tau_s s + 1)$; derivative control path, $K_d s/(\tau_s s + 1)^2$, where $K_p = 65$, $K_d = 0{\cdot}008$, $\tau_s = 1/(2\pi \times 5000)$; power amplifier DC gain = 1; sensor gain $\xi = 200$; rotor spin rate $\Omega = 17\,000$ rpm; shaking voltage frequency 200 Hz.

4.1. SIMULATION WITH LINEAR MODEL

Results for the linear model are shown in Table 2. It can be seen that the radius of the orbit at node 2 is proportional to the magnitude of the shaking voltage. The magnitude of the shaking voltage increases linearly with time until it reaches the desired steady state value. Figure 5 shows a linear system shaking orbit and power amplifier voltage for $V_{shaking} = 80$ V.

4.2. SIMULATION WITH NON-LINEAR MODEL

In the non-linear model, we include the non-linear magnetic bearing forces, the non-linear electric load expression and the saturation of the flux density. Table 3 summarizes the simulation results.

Figure 6 shows a shaking orbit and power amplifier voltage for the fully non-linear model when $V_{shaking} = 46$ V. Note that the target of 0·25 mm could not be achieved with a PD control. This was true even over an exhaustive range of K_p and K_d values.

5. FUZZY LOGIC CONTROL

From the simulation results, it can be seen that with the linear model, the radius of the shaking orbit can be easily made greater than 0·25 mm. For the non-linear model, the

TABLE 2

Linearized model forced response results

$V_{shaking}$	Radius of orbit at node 2 (mm)	Power amplifier voltage (V)	Power amplifier current (A)
20	0·0889	50	16
45	0·2032	110	35
80	0·3556	180	62

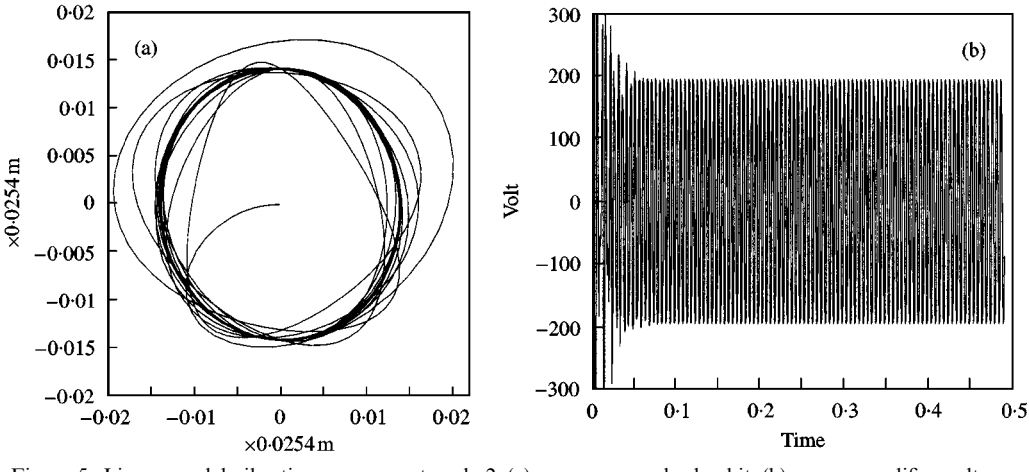

Figure 5. Linear model vibration response at node 2: (a) compressor wheel orbit; (b) power amplifier voltage.

TABLE 3

Simulation results for non-linear model with PD controllers

$V_{shaking}$ (V)	Radius of orbit at node 2 (mm)	Power amplifier voltage (V)	Power amplifier current (A)
20	0·0635	17	5
30	0·0965	25	8
45	0·1524	40	12
46	0·1549	46	14
50	Diverge		

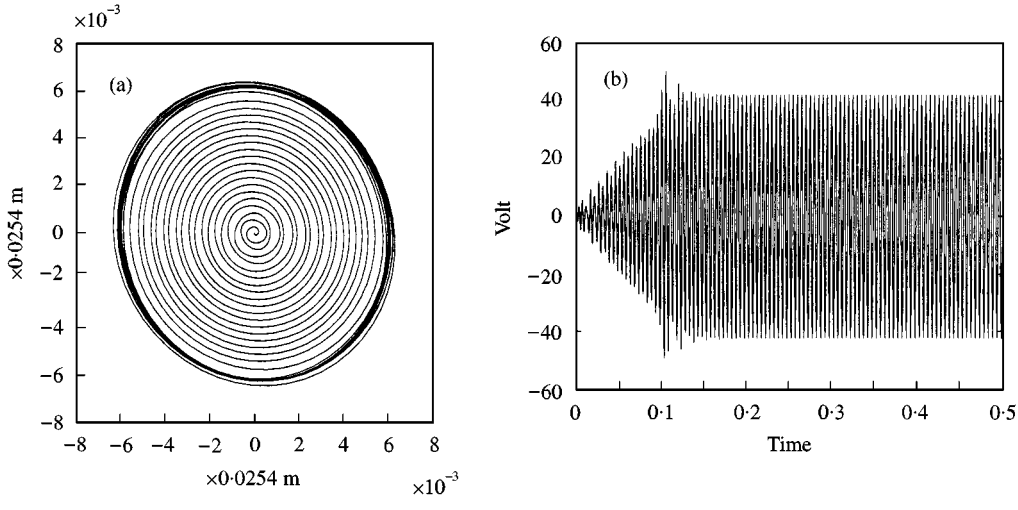

Figure 6. Nonlinear model vibration response at node 2 with PD control: (a) compressor wheel orbit; (b) power amplifier voltage.

maximum radius is 0·16 mm at a shaking voltage of 46 V. Further increase of the shaking voltage leads to system divergence.

For the active stall control studies, it is desired to obtain a shaking radius of 0·25 mm to reduce the stall of the compressor wheel. This target cannot be attained with the PD controller. A fuzzy logic controller is introduced in the control loop to overcome this difficulty. The 0·25 mm shaking radius can be reached by adding fuzzy logic controllers with Mamdani architecture.

Fuzzy logic is an intuitive way to map an input space to an output space. In our case, the input space is position voltage v_p and the rate of change voltage v_d, and the output space is the control voltage v_c. To employ a fuzzy logic controller, we define input and output membership functions which describe the truth of any statement as a matter of degree. More precisely, a membership function is a curve that defines how each point in the input space is mapped to a membership value between 0 and 1. Then based on experts' heuristic knowledge about how to control a system, a rule base is formulated holding the knowledge of how to best control the system.

The fuzzy logic controller is formed as follows. The 2 inputs called v_p and v_d, and one output denoted as v_c. Triangular and trapezoidal shapes are used to define the membership

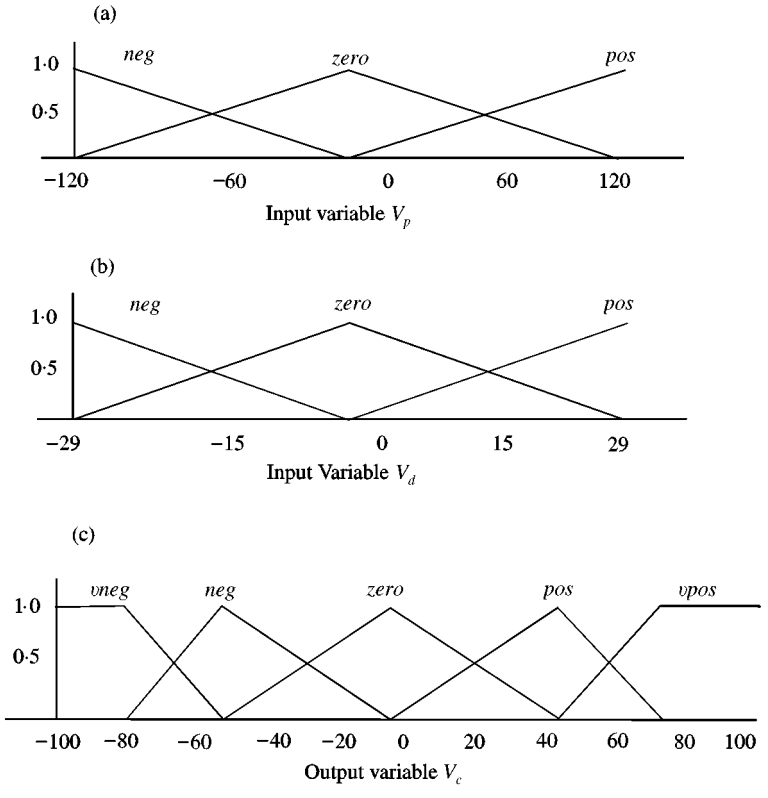

Figure 7. Input and output membership functions: (a) input membership function V_p; (b) input membership function V_d; (c) output membership function V_c.

TABLE 4

Rule base of fuzzy logic controller

Inputs	v_p: *neg*	v_p: *zero*	v_p: *pos*
v_d: *neg*	*vneg*	*neg*	*zero*
v_d: *zero*	*neg*	*zero*	*pos*
v_d: *pos*	*zero*	*pos*	*vpos*

functions. The 3-input membership functions for v_p are: *neg*, *zero*, *pos*. The 3-input membership functions for v_d are: *neg*, *zero*, *pos*. The 5-output membership functions for v_c are: *vneg*, *neg*, *zero*, *pos*, *vpos*.

Figure 7 depicts the input and output membership functions.

The rule base can be described in a compact form as shown in Table 4. Table 4 formulates 9 rules. For example, the first rule is

if v_p *is neg and* v_d *is neg, then* v_c *is v neg.*

Schematically, the closed-loop system with fuzzy logic controller is depicted in Figure 8.

The results with the fuzzy logic controller are shown in Table 5.

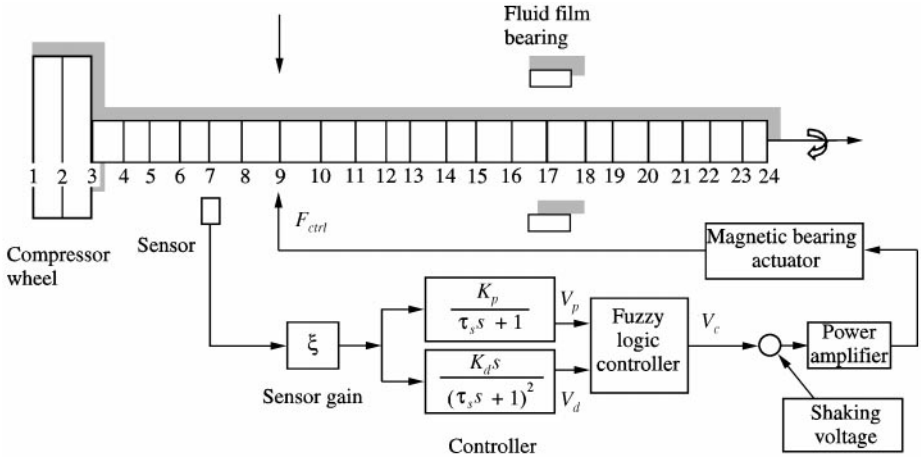

Figure 8. PD controllers with fuzzy logic control stage.

TABLE 5

Simulation results for non-linear model with fuzzy logic controllers

$V_{shaking}$ (V)	Radius of orbit	Power amplifier volt. (V)	Power amplifier current (A)
45	0·25 mm	220	70

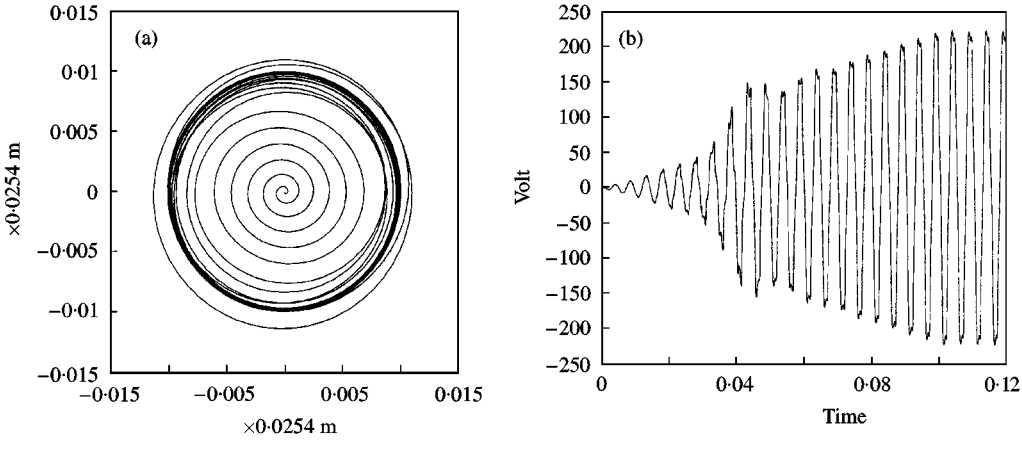

Figure 9. Shaking response with fuzzy logic control stage: (a) compressor wheel orbit; (b) power amplifier voltage.

It can be seen that the cost paid for the larger shaking radius is higher power amplifier voltage and current. However, these are within the allowable limits for the selected power amplifier. Figure 9 shows the wheel orbit and the power amplifier voltage with the fuzzy logic control stage.

6. CONCLUSION

In the closed-loop analysis, the frequency response with a shaking voltage of 66 V is given for the magnetic front bearing system. When the shaking frequency is 200 Hz, the shaking radius at node 2 reaches 0·29 mm with the designed PD control.

We have also shown that in the transient simulation, the linear model can reach a higher shaking orbit radius. When the shaking voltage is as high as 80 V, the simulation still converges and the orbit radius at node 2 is greater than 0·25 mm. However, the linearized force assumptions are shown to be invalid by comparing the results between the linear and non-linear models.

For the full non-linear case it is impossible to reach a 0·25 mm radius with conventional PD controllers. Further increase of the shaking voltage will result in simulation divergence. However, the large shaking amplitudes required for the NASA stall-rig necessitates a fully non-linear model. Although a linear approach can be used as a preliminary means to analyze the system, it is not appropriate for obtaining accurate results. By employing a fuzzy expert system, it has been shown that the shaking orbit radius may be increased to be 50% greater than that obtained with the conventional PD controllers. The fuzzy rule base system used in this approach is very simple and direct, so it is easy to implement on a real-time basis.

REFERENCES

1. C. KIM, A. B. PALAZZOLO, A. KASCAK and G. BROWN 1995 *Transactions of the ASME* **117**, 162–170. Eddy current effects on the design of rotor-magnetic bearing systems.
2. H. JEONG, C. KIM and C. LEE 1994 *Proceedings of the 4th International Symposium on Magnetic Bearings*, 23–28. Modeling and control of cone-shaped active magnetic bearing system.
3. F. MATSUMURA and T. YOSHIMOTO 1986 *IEEE Transactions Magnetics* **MAG-22**, 196–203. System modeling and control design of a horizontal shaft magnetic bearing system.
4. Y. ZHURAVLYOV 1998 *Proceedings of the 6th International Symposium on Magnetic Bearings*, 587–596. Linear quadratic optimal control of active magnetic bearings for high speed rotor.
5. K. NONAMI and T. ITO 1994 *Proceedings of 4th International Symposium on Magnetic Bearings*, 73–78. μ-Synthesis flexible rotor magnetic bearing control.
6. F. CARRERE, S. FONT and G. DUC 1994 *Proceedings of the 4th International Symposium on Magnetic Bearings*, 65–72. H_∞ control design of flexible rotor magnetic bearings.
7. M. FUJITA, K. HATAKE and F. MATSUMURA 1993 *IEEE Control System Magazine* **13**, 57–65. Loop shaping based robust control of a magnetic bearing.
8. F. MATSUMURA, T. NAMERIKAWA, K. HAGIWARA and M. FUJITA 1996 *IEEE Transactions on Control Systems Technology* **4**, 484–493. Application of gain scheduled H_∞ robust controllers to a magnetic bearing.
9. L. ZADEH 1965 *Information and Control* **8**, 338–353. Fuzzy sets.
10. E. MAMDANI 1976 *International Journal of Man-Machine Studies* **6**, 669–678. Advances in the linguistic synthesis of fuzzy controllers.
11. K. TAGAKI and M. SUGENO 1985 *IEEE Transactions on Systems, Man, and Cybernetics* **15**, 116–132. Fuzzy identification of systems and its application to modeling and control.
12. H. KOSKINEN, O. LINDGREN and O. KARASTI 1994 *Proceedings of the 4th International Symposium on Magnetic Bearings*, 89–93. Fuzzy logic in active magnetic bearing control.
13. B. WEIDEMANN and W. XIAO *Proceedings of the 4th International Symposium on Magnetic Bearings*, 59–64. A nonlinear fuzzy control for magnetic bearings without pre-magnetization.
14. J. HUNG 1995 *IEEE Transactions on Industry Applications* **31**, 1492–1497. Magnetic bearing control using fuzzy logic.

APPENDIX A

Finite element model of stall-rig

No. of Element	DO	DI	E	G	RHO	LEN
1	$14 \times 25{\cdot}4$	0	2·07e10	6·9e11	7·8	$0{\cdot}7 \times 25{\cdot}4$
2	$14 \times 25{\cdot}4$	0	2·07e10	6·9e11	7·8	$0{\cdot}7 \times 25{\cdot}4$
3	$5{\cdot}25 \times 25{\cdot}4$	$3 \times 25{\cdot}4$	2·07e10	6·9e11	7·8	$1{\cdot}25 \times 25{\cdot}4$
4	$3{\cdot}75 \times 25{\cdot}4$	$1 \times 25{\cdot}4$	2·07e10	6·9e11	7·8	$1{\cdot}0 \times 25{\cdot}4$
5	$3{\cdot}75 \times 25{\cdot}4$	$1 \times 25{\cdot}4$	2·07e10	6·9e11	7·8	$1{\cdot}25 \times 25{\cdot}4$
6	$3{\cdot}75 \times 25{\cdot}4$	$1 \times 25{\cdot}4$	2·07e10	6·9e11	7·8	$0{\cdot}5 \times 25{\cdot}4$
7	$4{\cdot}25 \times 25{\cdot}4$	$1 \times 25{\cdot}4$	2·07e10	6·9e11	7·8	$5/8 \times 25{\cdot}4$
8	$8{\cdot}25 \times 25{\cdot}4$	$4{\cdot}8 \times 25{\cdot}4$	2·07e10	6·9e11	7·8	$2{\cdot}5 \times 25{\cdot}4$
9	$8{\cdot}25 \times 25{\cdot}4$	$4{\cdot}8 \times 25{\cdot}4$	2·07e10	6·9e11	7·8	$3{\cdot}0 \times 25{\cdot}4$
10	$8{\cdot}25 \times 25{\cdot}4$	$4{\cdot}8 \times 25{\cdot}4$	2·07e10	6·9e11	7·8	$0{\cdot}5 \times 25{\cdot}4$
11	$6{\cdot}20 \times 25{\cdot}4$	$4{\cdot}8 \times 25{\cdot}4$	2·07e10	6·9e11	7·8	$3{\cdot}0 \times 25{\cdot}4$
12	$6{\cdot}20 \times 25{\cdot}4$	$4{\cdot}8 \times 25{\cdot}4$	2·07e10	6·9e11	7·8	$3{\cdot}0 \times 25{\cdot}4$
13	$6{\cdot}20 \times 25{\cdot}4$	$4{\cdot}8 \times 25{\cdot}4$	2·07e10	6·9e11	7·8	$3{\cdot}0 \times 25{\cdot}4$
14	$6{\cdot}20 \times 25{\cdot}4$	$4{\cdot}8 \times 25{\cdot}4$	2·07e10	6·9e11	7·8	$2{\cdot}75 \times 25{\cdot}4$
15	$6{\cdot}20 \times 25{\cdot}4$	0	2·07e10	6·9e11	7·8	$5/8 \times 25{\cdot}4$
16	$3{\cdot}30 \times 25{\cdot}4$	0	2·07e10	6·9e11	7·8	$1{\cdot}75 \times 25{\cdot}4$
17	$3{\cdot}30 \times 25{\cdot}4$	0	2·07e10	6·9e11	7·8	$1{\cdot}5 \times 25{\cdot}4$
18	$3{\cdot}30 \times 25{\cdot}4$	0	2·07e10	6·9e11	7·8	$1{\cdot}75 \times 25{\cdot}4$
19	$7{\cdot}30 \times 25{\cdot}4$	0	2·07e10	6·9e11	7·8	$5/8 \times 25{\cdot}4$
20	$7{\cdot}30 \times 25{\cdot}4$	0	2·07e10	6·9e11	7·8	$5/8 \times 25{\cdot}4$
21	$3{\cdot}50 \times 25{\cdot}4$	0	2·07e10	6·9e11	7·8	$1{\cdot}25 \times 25{\cdot}4$
22	$3{\cdot}50 \times 25{\cdot}4$	0	2·07e10	6·9e11	7·8	$0{\cdot}75 \times 25{\cdot}4$
23	$8{\cdot}25 \times 25{\cdot}4$	0	2·07e10	6·9e11	7·8	$1{\cdot}25 \times 25{\cdot}4$

Note: DO = outer diameter, mm; DI = inner diameter, mm; E = Young's modulus, N/m^2; G = elastic shear modulus, N/m^2; RHO = mass density, kg/cm^3; LEN = length of element, mm; total number of elements:= 23; total number of nodes:= 24.